Soil Surface Energy and Water Budgets during a Monsoon Season in Korea

CLAUDIO CASSARDO

Department of General Physics "Amedeo Avogadro," University of Turin, Turin, Italy

SEON KI PARK AND BINDU MALLA THAKURI

Severe Storm Research Center, and Department of Environmental Science and Engineering, Ewha Womans University, Seoul, South Korea

DANIELA PRIOLO AND YING ZHANG

Department of General Physics "Amedeo Avogadro," University of Turin, Turin, Italy

(Manuscript received 17 September 2008, in final form 25 May 2009)

ABSTRACT

In this study, attention has been focused on the climatology of some variables linked to the turbulent exchanges of heat and water vapor in the surface layer during a summer monsoon in Korea. In particular, the turbulent fluxes of sensible and latent heat, the hydrologic budget, and the soil temperatures and moistures have been analyzed. At large scale, because the measurements of those data are not only fragmentary and exiguously available but also infeasible for the execution of climatologic analyses, the outputs of a land surface scheme have been used as surrogate of observations to analyze surface layer processes [this idea is based on the methodology Climatology of Parameters at the Surface (CLIPS)] in the Korean monsoonal climate. Analyses have been made for the summer of 2005. As a land surface scheme, the land surface process model (LSPM) developed at the University of Torino, Italy, has been employed, along with the data collected from 635 Korean meteorological stations. The LSPM predictions showed good agreement with selected observations of soil temperature. Major results show that, during the rainfall season, soil moisture in the first tenths of centimeters frequently exceeds the field capacity, whereas most of the rainfall is "lost" as surface runoff. Evapotranspiration is the dominant component of the energy budget, sometimes even exceeding net radiation, especially during the short periods between the precipitation events; in these periods, daily mean soil temperatures are about 28°C or even more. The Gyeonggi-do region, the metropolitan area surrounding Seoul, shows some particularities when compared with the neighboring regions: solar radiation and precipitations are lower, causing high values of sensible heat flux and soil temperatures, and lower values of latent heat flux and soil moistures.

1. Introduction

In the recent years, there has been a significant growth in the recognition of the importance of the correct representation of soil moisture, sensible and latent heat fluxes in large-scale hydrology, and climate modeling. Soil moisture has long been suspected to exert an important influence on predictions of short-term weather (Rind 1982; Yeh et al. 1984) and climate (Shukla and Mintz 1982; Eltahir 1998; Douville and Chauvin 2000) as well as on mesoscale circulation (Yan and Anthes 1988), especially during the warm season, when land–atmosphere interactions are stronger (Reed 1925; Namias 1952). The evolution of the atmospheric systems—from weather forecasting to climate—is a major concern of the mankind, and it has become mandatory to provide a detailed description of the physical processes occurring near the soil surface. The land surface is a critical component through its partitioning of solar radiation into sensible and latent heat fluxes; its redistribution of precipitation into evaporation, soil storage, groundwater recharge, or runoff; and its regulation of biogeochemical cycles with processes such as photosynthesis and respiration.

The latent heat flux is an important term governing the surface energy balance in the presence of water,

Corresponding author address: Claudio Cassardo, Department of General Physics "Amedeo Avogadro," University of Turin, Via Pietro Giuria 1, 10125 Turin, Italy.
E-mail: cassardo@ph.unito.it

DOI: 10.1175/2009JHM1101.1

because it links the energy and water budgets. In fact, latent heat flux represents the energy needed for the evapotranspiration process, which originates both from the evaporation of the bare soil and from the transpiration of the vegetation. Evapotranspiration is physically linked to the fraction of water contained in the upper layers of soil in which the plant roots are located. Evapotranspiration and soil moisture are thus both involved in the water budget. In the atmospheric domain, soil moisture is a lower boundary condition that rules the partitioning of energy in terms of sensible and latent heat fluxes (Dirmeyer et al. 2000). Wrong estimations of soil moisture could have a deep effect on the model predictions, leading to the wrong simulation of the surface layer evolution, and hence forecasts of cloud cover and precipitations, in both medium and short ranges, could be consequently affected (Dirmeyer 2000).

Despite these considerations, there are only few extensive experimental measurements of these variables carried out in the world that do not allow the correct estimation of the energy and water balances on a wide area and for a sufficiently long time. Although there are some very limited networks possessing continuous observations for one to two decades (Robock et al. 2000), the land surface variables, such as soil moisture, are not routinely observed. Satellites could be used to infer the surface soil moisture, but the deduction of the surface soil moisture is still at a preliminary stage; in any case, this technique can give neither measurements of deep soil moisture nor turbulent heat fluxes.

Estimating the values of soil variables by using a numerical model can alleviate this kind of problems, and several efforts have been made for modeling the soil moisture; among those, we can quote the Project for the Intercomparison of Land-Surface Parameterization Schemes (PILPS), in which soil moisture modeling has been a crucial component (Shao and Henderson-Sellers 1996). To this end, it has been demonstrated that the land surface variables in a limited-area model could be suitably initialized by employing an approach called the Climatology of Parameters at the Surface (CLIPS; see Cassardo et al. 1997, 1999; Balsamo 1999). The CLIPS is basically the output of a soil–vegetation–atmosphere transfer (SVAT) scheme (which is specifically the LSPM described in section 3), driven by the meteorological observations gathered at some meteorological stations. It can be used to investigate the climate of a region where real observations of land surface variables are lacking. Application of such an approach for a long period (e.g., several years) may create a climatological archive of land surface data over some selected areas. However, such an archive would be useful only when the model-generated variables are in good agreement with observations.

Some land surface variables, such as soil moisture and temperature, are important in regional climate and hydrology. They may be strongly influential in a region with monsoon climate, where most precipitation is concentrated in a rainy spell, especially on hydrologic forecasts, including surface runoff and flood. In Korea about 40%–65% of total precipitation occurs between June and August during the summer monsoon. Characteristics of surface variables, and corresponding energy and hydrologic budgets in a monsoon environment have seldom been investigated. In this study, aiming at a better understanding of the land surface energy and hydrologic budgets in a monsoon environment, the LSPM (land surface process model) is applied using the Korean data during a monsoon season, in which evaporative processes dominate and hydrologic quantities determine the surface budgets. Major goals of the present study include the following:

1) Simulation of key components in the energy and hydrologic budgets, and soil temperature and moisture in the Korean Peninsula during a monsoon season, characterized by a warm and humid climate with significant amount of rainfall.
2) Investigation of the characteristic response of the land surface energy budget distributions to different land surface types.
3) Intercomparison of the simulated surface variables (e.g., first layer of soil temperature) with some observations.

Section 2 describes the general features of the 2005 summer monsoon in Korea. A short description of the LSPM is given in section 3. Section 4 explains dataset, initialization, and data processing procedures. The LSPM sensitivity results with respect to soil variables and the LSPM validation against observations are discussed in section 5 and 6, respectively. Main results are shown in section 7, with a particular attention to the components of the energy and hydrologic budgets, and soil temperature, and moisture. Concluding remarks are given in section 8.

2. Case description

The Korean Peninsula is located in East Asia and is mostly affected by the East Asian monsoon from late June to early August. During summer in East Asia, a monsoon front is generated along the boundary between the maritime tropical air mass (moist and warm air from the North Pacific subtropical high) and the maritime polar air mass (moist and cold air from the

FIG. 1. Map of the South Korean geography (adapted from Google Maps).

Okhotsk high). This quasi-stationary monsoon front—called baiu in Japan, mei-yu in China, and changma in Korea, respectively—leads to the main rainfall in East Asia. After the monsoon boundary transits north of a given location, it is not uncommon for daytime air temperatures to exceed 32°C, with dewpoints values of 24°C or higher (Takao et al. 2001).

For discussions on the characteristics of precipitation distribution, a geographical designation in the Korean Peninsula is necessary, as shown in Fig. 1. Here ''sanmaek'' is Korean for mountain range (hereafter MR)—for example, ''Taebaeksanmaek'' on the map means ''Taebaek MR.'' The Taebaek MR, the pivotal MR in Korea, lies in parallel to the eastern coast with an orientation from north-northwest to south-southeast. Other major MRs—mostly with an orientation from northeast to southwest—include the Sobaek, Noryeong, Charyeong, and Gwangju, from south to north.

In Fig. 2, the 2005 June–August mean 500-hPa maps are shown. It shows that a westerly flow, driven by the western North Pacific subtropical anticyclone, is predominant. During June 2005 (Fig. 2a), the western North Pacific subtropical anticyclone is weak, but it begins to strengthen. In July (Fig. 2b) and August (Fig. 2c), it gradually takes the control of the whole Korean Peninsula, causing stronger western currents and curving the flow from west to southwest in August. In these two months, as well as at the end of June, the accumulated rainfall is very large, especially in August.

Figure 3 depicts the monthly cumulative precipitation amount interpolated using the 635 station data (described

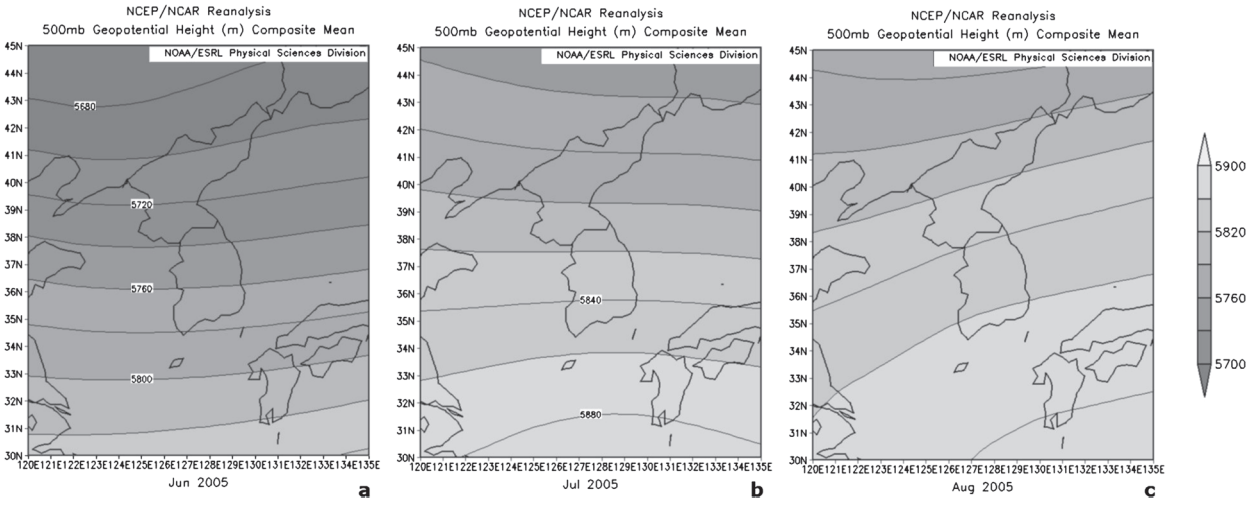

FIG. 2. Map of geopotential height at 500 hPa, provided by the National Oceanic and Atmospheric Administration/Earth System Research Laboratory (NOAA/ESRL) Physical Sciences Division, Boulder Colorado, from their Web site (available online at http://www.cdc.noaa.gov/) for (a) June, (b) July, and (c) August of 2005.

in detail in section 4) with the kriging model[1] of R (see details in http://www.r-project.org/).[2] In each month, some specific areas show larger amount of rainfall than others. Precipitation in June (Fig. 3a), which occurs mostly during the last 10 days, peaks (300 mm) near Hoengseong, in a closed basin bounded by the Charyeong MR to the south and the Gwangju MR to the north; on the contrary, the western coastal area at about 35.8°N (Honam Plain) and about all of the eastern coastal area south of 37°N show the lowest precipitation rates (100–150 mm).

In July, the largest precipitation (exceeding 400 mm) is observed over the Honam Plain and the Noryeong MR (Fig. 3b), located upwind to the western flow, with a weak convergence of the 500-hPa flow. A consistent amount of rainfall (300–400 mm) occurs at the western side of the Charyeong MR, whereas the lowest precipitations appear at the extreme southwestern coastal area and the inland area of the southwestern part of the peninsula (near Daegu), perhaps in orographic shadow.

Lastly, in August, the precipitation peak (500 mm) occurs in the metropolitan area near Seoul. Other areas receiving relevant rainfalls exist near the Charyeong and Noryeong MRs. These regions are located upwind of the southwestern flows at low level (not shown), revealing a local orographic rainfall enhancement. For the same reason, the eastern coastal area from Yeongdeok to Sokcho, being on the lee of the Taebaek MR, shows lower precipitation.

3. Model description

The LSPM has been developed at the University of Turin since 1990 with the aim of studying the land–atmosphere water and energy exchanges, as required in weather simulations and predictions (Cassardo et al. 1995). It is a one-dimensional model capable of analyzing and determining the energy, momentum, and water exchanges between the atmosphere and the land, and it can be used as a stand-alone model or coupled with mesoscale models (Cassardo et al. 2002a,b).

The land surface processes in the LSPM are described in terms of the physical and hydrological processes. Physical processes include radiative fluxes, momentum flux, sensible and latent heat fluxes, heat transfer in a multilayer soil or lake, partitioning of latent heat flux into canopy and soil evaporation, and transpiration. Hydrological processes include snow accumulation and melting, rainfall, interception, infiltration and runoff, and soil hydrology, including the water transfer in a multilayer soil. The user can choose the number and depths of the soil layers. In this study, seven soil layers are selected with thickness of 5, 10, 20, 40, 80, 160, and 320 cm, respectively, from top to bottom. The radiative fluxes include absorption, reflection, and transmittance of solar radiation, and absorption and emission of

[1] The kriging model assumes that the unknown function is a realization of Gaussian random spatial processes. The assumed model is additive $Y = P(x) + Z(X) + e$, where P is a low-order polynomial and Z is a mean zero, a Gaussian stochastic process with a covariance that is unknown up to a scale constant. See more details in Cressie (1991).

[2] R is a software for statistical computing and graphics; R provides a wide variety of statistical (linear and nonlinear modeling, classical statistical tests, time series analysis, classification, clustering, among others) and graphical techniques.

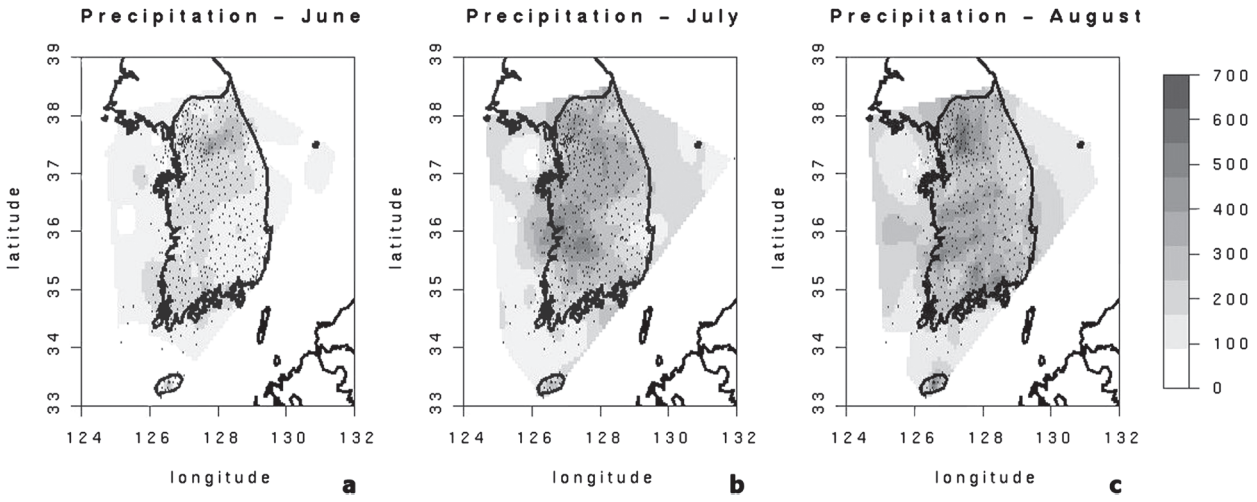

FIG. 3. Map of monthly cumulated precipitation according with the measurements carried out by the KMA meteorological stations for (a) June, (b) July, and (c) August of 2005.

longwave radiation. Momentum flux, and sensible and latent heat fluxes in the surface layer are based on the Monin–Obukhov similarity theory and parameterized with the resistance formulation. In particular, the canopy resistance formulation in the LSPM depends on solar radiation, air and soil moisture, and air temperature, following Chen et al. (1996).

More specifically, regarding the heat and water transfer into soil, the energy balance for the ith soil layer is

$$(\rho c)_i \frac{\Delta z_i}{\Delta t}(T_i^{n+1} - T_i^n) = -F_{z,i-1} + F_{z,i}, \tag{1}$$

where the superscripts n and $n + 1$ indicate the values at the beginning and end of the time step Δt, respectively, ρc is the soil heat capacity, Δz is the soil depth, T is the soil temperature, and F_z is the soil flux. The water balance for the ith layer is

$$\frac{\Delta z_i}{\Delta t}(\eta_i^{n+1} - \eta_i^n) = -Q_{i-1} + Q_i - e_i, \tag{2}$$

where η is the volumetric soil moisture content (volume of water per volume of soil), Q is the soil moisture flux, and e is the transpiration and surface evaporation. Both of these equations are solved using the Crank–Nicholson method. The internal time step of the LSPM for this study is set to 30 s, whereas the output data are saved every 30 minutes.

Regarding evaporation flux $E_f = E_{\text{trtot}} + E_{fw}$, neglecting the snow cover, the transpiration E_{trtot} is evaluated by

$$E_{\text{trtot}} = \rho_a s_{f\text{dry}}[q_{\text{sat}}(T_f) - q_{af}]\sigma_f, \tag{3}$$

where ρ_a is the air density, $s_{f\text{dry}}$ is the ''dry'' canopy conductance (accounting for both canopy resistance and laminar boundary layer resistance—the former is not considered in case of condensation), $q_{\text{sat}}(T_f)$ is the saturated specific humidity at the canopy temperature T_f, q_{af} is the air within canopy temperature, and σ_f is the vegetation cover. Evaporation or condensation involving the wet portion of the leaves E_{fw} is expressed by

$$E_{fw} = \rho_a s_{f\text{wet}}[q_{\text{sat}}(T_f) - q_{af}]\sigma_f, \tag{4}$$

in which $s_{f\text{wet}}$ is the ''wet'' canopy conductance. Bare soil evaporation E_g is given by

$$E_g = \rho_a s_s[f_h q_{\text{sat}}(T_1) - q_{af}](1 - \sigma_f), \tag{5}$$

where s_s is the soil conductance (accounting for soil surface resistance and air-within-canopy resistance—the former is not considered in the case of condensation) to the evaporation and T_1 is the surface soil temperature. For a detailed description of the LSPM physics, refer to Cassardo (2006).

The model validation has been carried out using experimental datasets gathered in Italy (Cassardo et al. 1998, 2002a,b, 2006a,b, 2007), in some European stations (Ruti et al. 1997; Cassardo et al. 2005), in Sahel (Qian et al. 2001), in the Gobi desert (Feng et al. 1997), and over the ice shelf of Antarctica (Cassardo et al. 2002c).

4. Initialization, dataset, and data processing

To run the LSPM properly, the initial and boundary conditions are required and thus some data processing is necessary. The Korean Meteorological Administration (KMA) maintains about 760 meteorological stations distributed almost regularly within the peninsula and the

main inhabited islands, with its greatest station density in the Gyeonggi-do region, surrounding Seoul. For this study, the observational data of these KMA stations, from 1 June to 31 August in 2005, have been used for the simulation. Because the LSPM requires complete data for input, some station data with missing variables are interpolated from other station data. For some stations, almost all variables may be missing at specific observation times, resulting in most of their data being interpolated. By excluding such stations in which most data are obtained through interpolations, a special dataset has been created for 635 stations containing temperature, pressure, relative humidity (RH), wind speed, precipitation, and solar radiation (see section 4b for the details of the preprocessing). Only stations with a relevant number of observations were considered (to not have stations in which most of their data were interpolated). Thus the total number of stations used for the simulations decreased to 635.

Some additional observations of soil temperatures collected from 76 KMA stations are used for the validation of the model simulations.

Data processing includes the preprocessing of input data and postprocessing of output data. The preprocessing mainly includes spatial and temporal interpolations for missing data because the model requires a continuous dataset. The postprocessing consists of calculation of daily and monthly-mean or cumulative values (for hydrological variables) of the model output. These variables include components of energy balance (net radiation, sensible heat flux, latent heat flux , conductive fluxes over vegetated and bare soil) and hydrologic budget (evapotranspiration, surface runoff, and underground drainage), and soil temperature and moisture.

a. Initialization of soil temperature and moisture

One of the most important tasks in using the LSPM is the initialization of soil temperature and moisture, especially for short-term simulations. Wrong initial values of these variables would produce the so-called spin-up problem; that is, the initial over or underestimation may last even several months, and the amplitude is related to the initial error in the soil temperatures and, particularly, soil moistures (see, for instance, Koster and Suarez 2001). For this reason, two formulations, reported in Cassardo et al. (2006b), are applied to the Korean stations to estimate the initial values of soil temperature and moisture (Malla Thakuri 2007; Priolo 2007).

If the air temperature observations referring to one year are available, then the initial value of soil temperature $T_{\mathrm{emp}}(z, t)$ at the soil depth z and time t can be estimated in the function of the daily mean air temperature T_{air} as

$$T_{\mathrm{emp}}(z, t) = T_{\mathrm{air}} + \Delta T_{\mathrm{exc}} \exp\left(-\frac{z}{D}\right) \sin\left(\frac{2\pi J}{365} - \frac{z}{D} + \phi\right), \tag{6}$$

where $\Delta T_{\mathrm{exc}} = T_{\mathrm{July}} - T_{\mathrm{January}}$ is the annual thermal excursion (in the air), J is the day angle and D (=2.3 m for loam) is the depth of exponential decay for temperature.

The initial value of soil moisture $q_{\mathrm{emp}}(z, t)$ at z and t, expressed in units of saturation ratio, can be estimated as a function of the daily mean relative humidity $\mathrm{RH}_{\mathrm{air}}$ using an attenuation of the surface amplitude similar to Eq. (6):

$$q_{\mathrm{emp}}(z, t) = q_{\mathrm{fc}} - (q_{\mathrm{fc}} - q_{\mathrm{wi}})\left(\frac{\mathrm{RH}_{\mathrm{max}} - \mathrm{RH}_{\mathrm{air}}}{\mathrm{RH}_{\mathrm{max}} - \mathrm{RH}_{\mathrm{min}}}\right) \times \exp\left(-\frac{z}{D}\right), \tag{7}$$

where q_{wi} and q_{fc} are the wilting point and the field capacity, respectively, both expressed in units of saturation ratio ($\mathrm{m}^3\ \mathrm{m}^{-3}$), and $\mathrm{RH}_{\mathrm{max}}$ (=90%) and $\mathrm{RH}_{\mathrm{min}}$ (=65%) are empirical thresholds (Cassardo et al. 2006b). To avoid unrealistic values for q_{emp}, the function of $\mathrm{RH}_{\mathrm{air}}$ must be always limited between 0 and 1.

In this study, only three months of observed air temperature were available, thus the annual thermal excursion of each site was estimated roughly by assuming that daily air temperature has a sinusoidal trend with its maximum on 5 August (this assumption means that, being $z = 0$ and $J = 217$, $2\pi(217/365) + \phi = \pi/2$, from which $\phi = 1.245$ rad = 71.34°). In this way, using the mean air temperatures of June [T_{Jun}, associated with the central day of the month (15 June)—i.e., $J = 166$] and August (T_{Aug}, associated with 15 August—i.e., $J = 227$) as a surrogate of the values at the level $z = 0$, the annual temperature excursion was estimated by evaluating $T_{\mathrm{Aug}} - T_{\mathrm{Jun}} = T_{\mathrm{emp}}(0, 15\ \mathrm{August}) - T_{\mathrm{emp}}(0, 15\ \mathrm{June})$. Using Eq. (6), $T_{\mathrm{Aug}} - T_{\mathrm{Jun}} \approx T_{\mathrm{Aug}} + \Delta T_{\mathrm{exc}} \sin(99.86°) - T_{\mathrm{Jun}} - \Delta T_{\mathrm{exc}} \sin(39.70°)$, which, solved for ΔT_{exc}, gives

$$\Delta T_{\mathrm{exc}} \approx \frac{T_{\mathrm{Aug}} - T_{\mathrm{Jun}}}{\sin(99.86°) - \sin(39.70°)}. \tag{8}$$

b. Preprocessing of data

Because the LSPM requires as input a complete (i.e., without missing data) file for every station, the missing data for every station have been interpolated.

Moreover, the original data rate of one observation per hour has been stepped out at the rate of a datum per half hour. Two kinds of interpolation methods have been used—spatial and time interpolation. The spatial interpolation has been used only in case of data missing for a period longer than four hours, and employed the inverse square distance method in which all n observations ϕ_j, included in a maximum circle of 250 km surrounding the target station, has been considered. The formula is

$$\phi_i = \frac{\sum_{j=1}^{n} \frac{\phi_j}{r_{ij}^2}}{\sum_{j=1}^{n} \frac{1}{r_{ij}^2}}, \tag{9}$$

where ϕ_j is the variable measured in the jth station, ϕ_i is the variable evaluated in the ith target station, and r_{ij} is the distance between the ith and jth stations.

Pressure and temperature data, being strongly dependent on elevation, have been previously scaled with the altitude difference ΔZ among ith and jth stations, according to the expressions

$$p'_j = p_j \exp\left(-\frac{\Delta Z}{H_{\text{ref}}}\right) \quad \text{and} \tag{10}$$

$$T'_j = T_j - \gamma \Delta Z, \tag{11}$$

where $H_{\text{ref}} = 8000$ m is the height scale (hydrostatic approximation) and $\gamma = 0.6$ K km^{-1} is the standard atmosphere lapse rate.

In regard to the temporal interpolation, if $\phi(t_1)$ and $\phi(t_2)$ are the valid observations at two times t_1 and t_2, t_1 and t_2 corresponding to the last valid observation before the missing data and to the first valid observation after the missing data, respectively, and $t_2 - t_1 < 4$ h, the missing observation $\phi(t)$ at t has been interpolated as

$$\phi(t) = \phi(t_1) + \frac{\phi(t_2) - \phi(t_1)}{t_2 - t_1}(t - t_1). \tag{12}$$

Such a preprocessing procedure has enabled the building of a dataset, composed of 635 stations, in which all input data required by the LSPM during the 2005 summer period were available every 30 minutes.

c. Dataset for the vegetation parameters

The LSPM can initialize the vegetation parameters in the following three ways:

1) giving the specific values for each parameter;
2) taking the values from an extension (Cassardo 2006) of the global dataset of Wilson and Henderson-Sellers (1985)—in this case, only the vegetation code is required;
3) taking the values from the Ecoclimap database (Masson et al. 2003).

For this experiment, the values of the extended global dataset of Wilson and Henderson-Sellers (1985) have been used (see Table 1).

To assign a particular vegetation code at a given location, the Kongju National University (KNU) land cover (KLCV) database, derived from the 3-yr Moderate Resolution Imaging Spectroradiometer (MODIS), has been used. This database classifies the land use of Korea into 10 classes, as reported in Table 1. The KLCV database comprises 700 × 1100 points in a rectangular portion (32.80°–43.24°N in latitude and 123.50°–132.39°E in longitude), centered over the Korean Peninsula with an average grid size of about 1.5 km. For each station the land-use type of the nearest KLCV grid point has been selected. A correction has been made for all stations in which this algorithm has assigned as vegetation type ''water body,'' perhaps as a result of their vicinity to the seal; in all these cases, the vegetation type has been reassigned to another value.

Among the 635 considered stations (The statistics for the land-use type is reported in Table 1.), the most frequent land-use types are dry land cropland and pasture (32%), and mixed forest (16%). The vegetation types selected with this procedure show a better agreement with the vegetation maps of Korea (see, for instance, Park et al. 2003) than those of the ECOCLIMAP database.

d. Dataset for the soil parameters

Soil parameters are taken from an extension of the Clapp and Hornberger (1978) database (see Table 2); the parameters are classified by soil type code, an index that needs to be specified externally and that subdivides the soil according to its percentage of clay (diameter $d < 2$ μm), silt (2 μm $< d <$ 0.05 mm) and sand (0.05 mm $< d <$ 2 mm), d being the diameter of soil grains, according to the U.S. Department of Agriculture (USDA) Natural Resources Conservation Service's (NRCS) soil textural database.

To deduce the soil type characteristics for each station, the percentages of sand and clay have been extracted from the Ecoclimap database, which are in turn taken from the Food and Agriculture Organization (FAO) information source (at 10 km of resolution; FAO 1988). Using these data, the soil type code has been evaluated for each station. Among the 635 considered stations (The statistics for the land-use type is reported in Table 2.), the most frequent soil type is loam (64%).

For each station, the soil has been subdivided into seven layers whose depths were progressively larger. The depths are 5, 10, 20, 40, 80, 160, and 320 cm, respectively, from the surface layer to the deepest, with a total of 6.35 m.

TABLE 1. Vegetation types characteristics. WHS column from 1 to 18 indicates codes taken from Wilson and Henderson-Sellers (1985); from 19 to 23 are codes taken from Cassardo (2006). Vegetation type column is the vegetation cover associated with column 1 (and 2). The variables are: α_f is the albedo (lw refers to longwave and sw for shortwave), h_f is the vegetation height, R_{gl} is the Noilhan parameter for the dependence of canopy stomatal resistance from solar radiation, r_{min} is the minimum stomatal resistance, d_f is the leaf dimension, $\sigma_{f\text{sum}}$ is the base vegetation cover, $\Delta\sigma_f$ is its seasonal variation, LAI_{min} is the winter value of leaf area index, and ΔLAI is its annual excursion. Notice that the value of KLCV corresponding to inland water (1) corresponds to WHS code 14; however, in this study, it has been associated with WHS code 1 because it was referring to stations over small islands.

WHS	KLCV	Vegetation type	α_f (lw)	α_f (sw)	h_f	R_{gl}	r_{min}	d_f	$\sigma_{f\text{sum}}$	$\Delta\sigma_f$	LAI_{min}	ΔLAI
1	4	Crop and mixed farming	0.05	0.2	0.8	100	120	10	0.85	0.6	6	5.5
2	10	Short grass	0.04	0.26	0.5	100	200	5	0.8	0.1	2	1.5
3	6	Evergreen needleleaf tree	0.03	0.1	10	30	200	5	0.8	0.1	6	1
4	—	Deciduous needleleaf tree	0.05	0.1	10	30	200	5	0.8	0.3	6	5
5	5	Deciduous broadleaf tree	0.05	0.2	8	30	200	5	0.8	0.3	6	5
6	7	Evergreen broadleaf tree	0.05	0.15	20	30	150	5	0.9	0.5	6	1
7	—	Tall grass	0.04	0.16	1	100	200	5	0.8	0.3	6	5.5
8	—	Desert	0.14	0.3	0.5	100	200	5	0	0	0	0
9	—	Tundra	0.05	0.2	0.4	100	200	5	0.6	0.2	6	5.5
10	3	Irrigated crop	0.15	0.18	0.6	100	200	5	0.8	0.6	6	5.5
11	—	Semidesert	0.04	0.25	1	100	200	5	0.35	0.1	6	5.5
12	—	Ice cap/glacier	0.18	0.4	0.1	100	200	5	0	0	0	0
13	—	Bog or marsh	0.02	0.12	0.3	100	200	5	0.8	0.4	6	5.5
14	1(*)	Inland water	0.01	0.14	0	100	200	5	0	0	0	0
15	—	Ocean	0.01	0.14	0	100	200	5	0	0	0	0
16	—	Evergreen shrub	0.03	0.1	1	60	200	5	0.8	0.2	6	1
17	9	Deciduous shrub	0.03	0.2	1	60	200	5	0.8	0.3	6	5
18	8	Mixed woodland	0.04	0.18	8	60	200	5	0.8	0.2	6	3
19	2	Settlement	0.03	0.16	5	100	200	5	0.1	0.1	6	3
20	—	Dense settlement	0.02	0.17	10	100	200	5	0	0	0	0
21	—	Po Valley [San Pietro Capofiume (SPC)]	0.04	0.28	0.05	100	100	5	1	0.2	2	1.5
22	—	Grugliasco	0.04	0.2	2	100	50	10	0.8	0.4	6	5.5
23	—	Siberia	0.04	0.25	0.09	100	100	5	0	0	0	0

e. Postprocessing of output data

After these preliminary preprocessing operations, the simulations have been carried out with the LSPM. Subsequently, among all the LSPM output values, databases containing the daily and monthly-mean values of the following variables have been created:

1) energy balance components (net radiation, sensible and latent heat fluxes, and conductive flux over

TABLE 2. Soil type characteristics. (left)–(right) The columns are defined as follows: first two columns are the soil codes and types, as indicated by Clapp and Hornberger (1978), for codes from 1 to 12, and by Cassardo (2006) for codes 13 and 14; b is a coefficient; $K_{\eta s}$ is the saturated hydraulic conductivity ($\text{dm}^2\ \text{s}^{-1}$); η_s is the porosity (in units of volumetric soil moisture); η_{wi} is the wilting point (in units of volumetric soil moisture); ψ_s is the saturated moisture potential (cm); and ρ_c is the dry soil heat capacity ($\mu\text{J}\ \text{m}^{-3}\ \text{K}^{-1}$). Perc indicates the percentage of stations as a function of the specific soil type code in Korea.

Code	Soil type	b	$K_{\eta s}$	η_s	η_{wi}	ψ_s	ρ_c	Perc
1	Sand	4.05	0.0176	0.395	0.0677	−12.1	1.465	0
2	Loamy sand	4.38	0.015 63	0.41	0.075	−9	1.407	0
3	Sandy loam	4.9	0.003 41	0.435	0.1142	−21.8	1.344	0
4	Silt loam	5.3	0.000 72	0.485	0.1794	−78.6	1.273	2
5	Loam	5.39	0.0007	0.451	0.1547	−47.8	1.214	64
6	Sandy clay loam	7.12	0.000 63	0.42	0.1749	−29.9	1.177	0
7	Silty clay loam	7.75	0.000 17	0.477	0.2181	−35.6	1.319	0
8	Clay loam	8.52	0.000 25	0.476	0.2498	−63	1.227	34
9	Sandy clay	10.4	0.000 22	0.426	0.2193	−15.3	1.177	0
10	Silty clay	10.4	0.0001	0.492	0.2832	−49	1.151	0
11	Clay	11.4	0.000 13	0.482	0.2864	−40.5	1.088	0
12	Peat	7.75	0.0008	0.863	0.3947	−35.6	2.094	0
13	Ice	3.2	0.031 79	0.355	0.0212	−4.8	1.911	0
14	Very pure sand	2	0.005 55	0.4	0.0677	−18	1.465	0

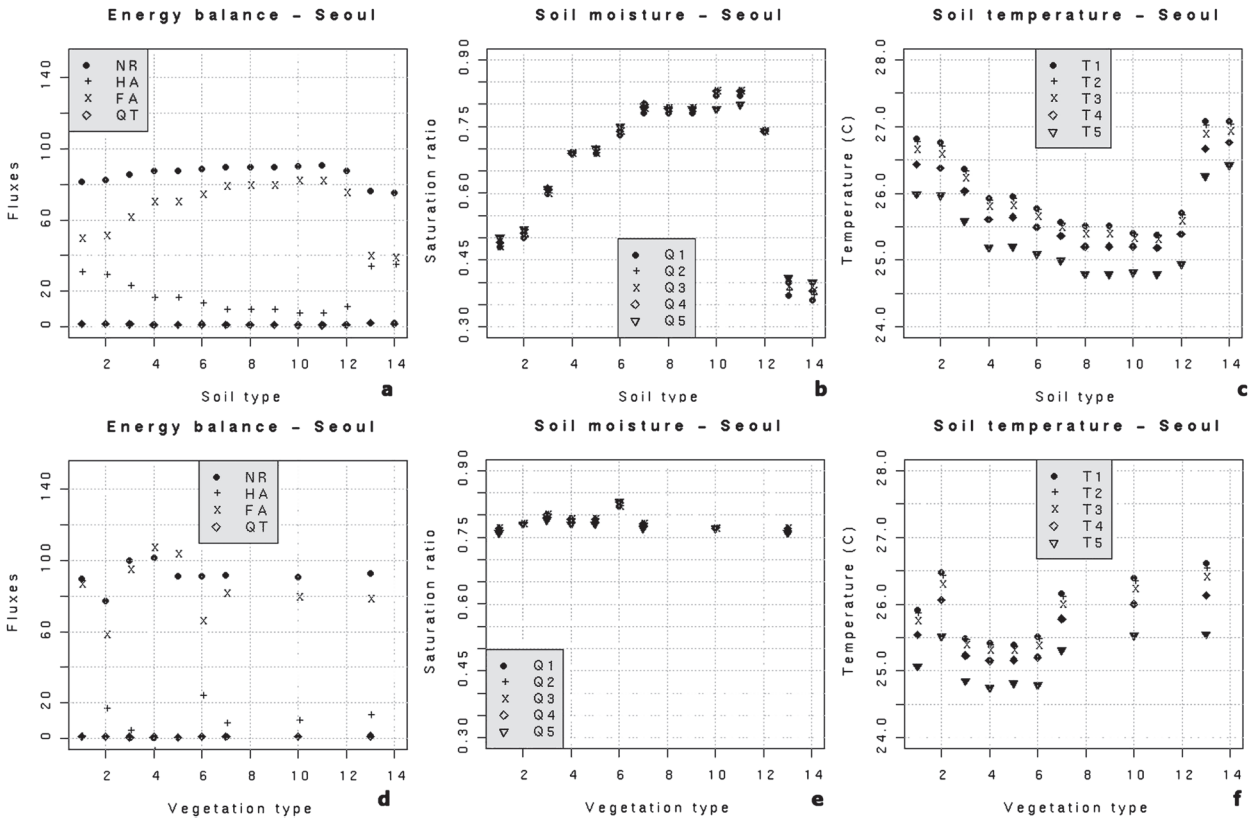

FIG. 4. LSPM outputs of the sensitivity experiment on the vegetation and soil type (whose codes—refer to Tables 1 and 2—are on the *x* axis). The vegetation codes are a selection of the 14 most meaningful vegetation types among the 23 vegetation types reported in the Table 1. On the abscissa, the codes for 1–7 are the same as Table 1 plus the following: 8, irrigated crops; 9, bog and marsh; 10, evergreen shrubs; 11, deciduous shrubs; 12, mixed woodland; 13, settlement; and 14, Po Valley (Italy). Data refer to August. (a) Energy balance components vs soil type: RN is net radiation, HA is sensible heat flux, FA is latent heat flux, and QT is the SVA heat flux (all components are expressed in W m^{-2}). (b) Humidity of the upper five soil layers vs soil type, expressed in units of saturation ratio. (c) Temperature of the upper five soil layers vs soil type, expressed in °C. (d) Energy balance components vs vegetation type. (e) Humidity of the upper five soil layers vs vegetation type. (f) Temperature of the upper five soil layers vs vegetation type.

vegetation and bare soil), plus the global radiation (input) for the sake of comparison;
2) hydrologic budget components (precipitation, evapotranspiration, surface runoff, and underground drainage) as well as the precipitation, which is the input data for this budget;
3) soil temperature and moisture.

5. Sensitivity of the LSPM to soil parameters

After the completion of the preprocessing and before carrying out the LSPM run over all stations, to check the correct performance of the LSPM, some simulations have been carried out over a significant station by varying the type of soil and vegetation. In fact, the choice of the proper soil and vegetation parameters is a key factor that influences the results of the simulations performed at single sites (Ek and Cuenca 1994; Xue et al. 1997).

For the sensitivity experiment on the soil types, the station of Seoul (KMA code = 108; vegetation type = settlement; soil type = clay loam), where the precipitation has been intense between the end of June and the end of August with a total of approximately 700 mm of accumulated rainfall, has been chosen as the experimental station. Then, 14 simulations have been carried out for 14 different soil type codes, using the same initial and boundary conditions. Similarly, 14 other simulations have been carried out by varying only the vegetation type code (for a total of 23 codes; see Table 1), excluding the codes 8, 9, 11, 12, 14, 15, 20, 22, and 23 that are not meaningful for this experiment.

Each simulation has lasted for three months. Output values have been averaged (or accumulated) on a monthly basis, and the monthly values of August have been examined.

Figure 4a shows the energy balance components. Net radiation and latent heat flux are larger for silty soils

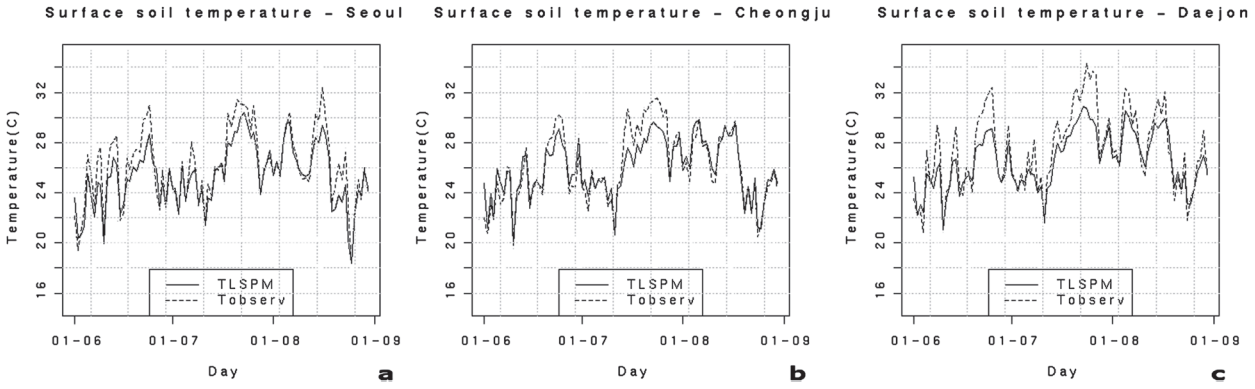

FIG. 5. Intercomparison between simulated and observed daily mean soil temperature in the first layer (5 cm) during summer 2005 (°C) at (a) Seoul, (b) Cheongju, and (c) Daejeon.

(codes 11 and 12) and smaller for sandy soils (codes 1, 2, 13, and 14). On the contrary, the sensible heat flux and the flux into the canopy and soil are larger for sandy soils and smaller for silty soils. These results seem physically reasonable and are in agreement with the behavior of other variables. For instance, sandy soils are less humid (The curves of soil moistures, shown in Fig. 4b, possess the same trend of those of latent heat flux.) and warmer (Fig. 4c). The low soil moisture content favors a higher soil albedo, thus increasing the reflected shortwave radiation. The higher soil temperature also favors the increment of the longwave radiation emitted by the soil surface. Both effects are combined to produce a decrease in the net radiation. For the partitions of the turbulent fluxes, a soil composed of fine sand drains the rainfall amount more effectively, maintaining lower surface soil moisture and thus producing larger values of the sensible heat flux.

The LSPM outputs also show sensitivity to the vegetation type. Trees (except for the evergreen broadleaf trees) have the highest net radiation (the lower albedo effect prevails over the higher canopy temperature effect), the smallest sensible heat flux (negative for the deciduous broadleaf trees), the highest latent heat flux (even larger than the net radiation for the deciduous trees), medium soil moistures, and the lowest soil temperatures. On the contrary, the lower vegetation and the evergreen broadleaf trees show the lowest net radiation, the highest sensible heat flux, the lowest latent heat flux, and the highest soil moisture. Other vegetation types show intermediate values. The settlement shows the absolute highest soil temperature and the absolute lowest soil moisture, but their effects almost compensate for what is occurring with the energy balance components, which show intermediate values.

In conclusion, through these sensitivity experiments, it is evident that the simulation of the energy budget significantly depends on the soil and vegetation types. For this reason, it is quite important to set up well the initial conditions at the beginning of the simulation; thus, special databases (KLCV for vegetation types and Ecoclimap for soil types) have been used for this study.

6. Validation of the LSPM

Figure 5 shows the temperatures of the first soil layer for some selected significant stations; the solid lines represent the daily average values of the LSPM results, whereas the dashed lines depict those of observations.

In some stations (e.g., Cheongju) the initial values of temperature, calculated from Eq. (6), appear to be overestimated in comparison with observations, whereas in some other stations (e.g., Seoul) the estimation errors are kept quite small and uniformly distributed. Generally, the largest difference in the daily mean values of temperature is about 2°C in most cases, both on sunny and cloudy days. In the majority of the stations, the warmest periods, from the last third of July to the first half of August, are accurately reproduced. The colder temperatures observed at the end of August, sometimes more regular (e.g., Daejeon) sometimes less (e.g., Seoul and Cheongju), are well simulated by the LSPM.

To get more quantitative information, a statistical analysis has been carried out on the comparison between the simulated and observed data. As shown in Table 3, the absolute value of bias is lower than 0.5°C in 37% of stations and lies in the range between 0.5° and 1°C in 31% of stations, whereas it is larger than 2°C only in 7% of stations. Generally speaking, the root-mean-square errors (rmse) and the correlation coefficients (Table 3) confirm that the LSPM is able to correctly reproduce the soil temperature of the first layer.

TABLE 3. Percentages (Perc) of bias (°C), rmse (°C), and square correlation coefficient (r^2) classes among LSPM simulated and observed daily mean soil temperatures for the upper soil layer (5 cm).

Bias classes	Perc	rmse classes	Perc	r^2 classes	Perc
$\lvert\text{bias}\rvert \le 0.5$	37	rmse ≤ 1	4	$r^2 \le 0.5$	0
$0.5 < \lvert\text{bias}\rvert \le 1$	31	$1 <$ rmse ≤ 2	68	$0.5 < r^2 \le 0.8$	75
$1 < \lvert\text{bias}\rvert \le 2$	25	$2 <$ rmse ≤ 3	21	$0.8 < r^2 \le 0.9$	21
$\lvert\text{bias}\rvert > 2$	7	rmse > 3	7	$r^2 > 0.9$	4

7. Results

A summary of the 635 simulations will be presented in two different ways. First, the time trends of the daily mean or accumulated values of variables will be presented for some selected stations to show the temporal variability of data. Second, the monthly mean or accumulated values of variables will be shown in maps over the Korean territory, showing the spatial variability of data.

a. Temporal variability in point stations

Among a large number of stations (635), choosing the most meaningful ones to be shown is hard. Thus, three stations have been chosen: two of them are representative of the areas most affected by rainfall: Jibyeon (KMA code = 3), located in the northeastern part of South Korea (hereafter SK), and Daejeon (KMA code = 133), located in the central western part; the third one is Seoul (KMA code = 108), located in the northwestern part of SK. The choice of Seoul has been made not because it is the capital city of Korea but because the values of variables and their trends are peculiar, as will be clearly seen in the next section.

The hydrologic budgets (Fig. 6) report the accumulated value of precipitation (which is an input for the LSPM), evapotranspiration, surface runoff, and underground drainage. The accumulated precipitation clearly shows the duration of the rain season, during which precipitations are discontinuous, depending on the station location. A careful analysis of the duration of the changma period (the rainy season) in SK has been carried out by looking at the precipitation data measured by KMA. It turned out that for most stations, monsoonal precipitations started at 26–28 June (92%) and ended at 24–25 August (91%).

Evapotranspiration peaks in the middle of July, during the relative pause of precipitations. This peak can be demonstrated by the increase in the slope of the cumulative curve or by the latent heat flux curves in Fig. 7. Among the three stations shown, evapotranspiration is particularly low in Seoul.

Surface runoff exceeds underground drainage and sometimes evapotranspiration (at Seoul and particularly at Daejeon, where surface runoff is about one-half of the precipitation), depending on the soil type. Underground drainage is the smallest component in almost every station.

The water budget—defined as precipitation minus the sum of evapotranspiration, surface runoff, and underground drainage—is strongly positive everywhere, which implies that the soil of every location gains water during summertime. Evidence of this assertion can be seen in the three stations of Fig. 8 by comparing the initial and final values of the soil moistures. It demonstrates that the abundant monsoonal precipitations effectively wet the soil in such a way that the soil itself can be considered a sort of ''water reservoir'' for the future months, in which generally precipitations are generally lower.

The trends of the daily averages of soil moisture (expressed in saturation ratio and shown in Fig. 8) in the upper six layers of soil (thicknesses discussed in section 3) show that, in relation to the beginning of the rain season,

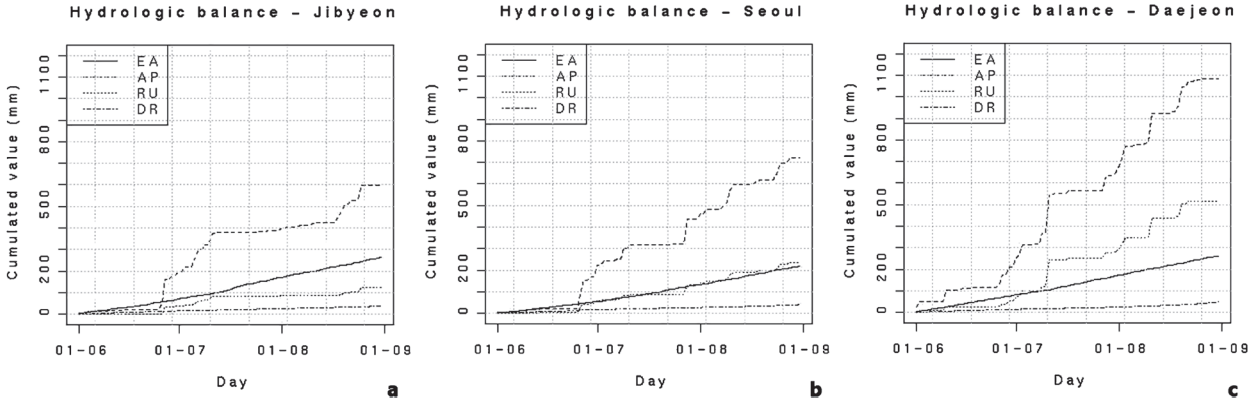

FIG. 6. Cumulated values of hydrological balance components during summer 2005 at (a) Jibyeon, (b) Seoul, and (c) Daejeon; EA = evapotranspiration, AP = precipitation, RU = surface runoff, and DR = underground drainage.

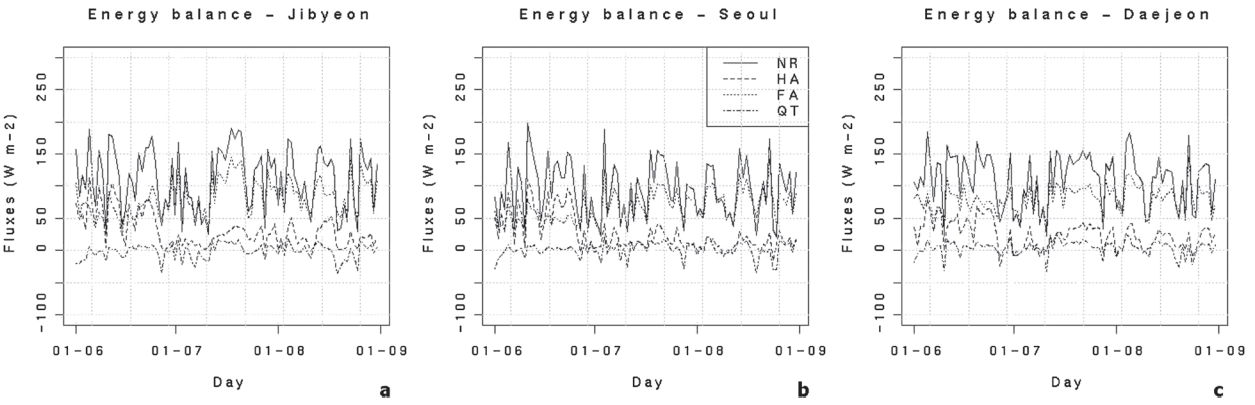

FIG. 7. Daily mean values of energy balance components (W m^{-2}) during summer 2005 at (a) Jibyeon, (b) Seoul, and (c) Daejeon.

the moisture in the first layer reaches high values, sometimes greater than the field capacity. It is particularly true in Seoul and Daejeon, where the first-layer moisture frequently exceeds the daily means of 0.85 (i.e., 85% of the saturation ratio). The inferior layers (e.g., the fifth layer, 75 cm deep and located 80 cm below the soil surface) are wetted with a delay of 5–7 days. After a rainfall episode, the soil moisture diminishes rapidly because of the very large hydraulic conductivity and also because of the high evapotranspiration. These results agree with the distribution of the latent heat flux (see Fig. 7).

In Jibyeon (Fig. 8a), in which soil type is silt loam, the surface soil moisture before the beginning of the rainy season is close to the wilting point (0.37, expressed in units of saturation ratio). During the intensive rainfall events on both 26–27 June and 18–21 August, the moisture in the upper three soil layers suddenly grows, exceeding the field capacity (0.76 for the silt loam soil).

At Seoul (Fig. 8b) the soil moisture at the beginning of June is low, and in the first soil layer (whose type is clay loam) it is lower than the wilting point (0.52 for clay loam); however, after the precipitation event on 26 June, the soil moisture increases, exceeding the field capacity (0.82). During August, the uppermost five soil layers (i.e., the highest 1.55 m of soil) have soil moisture close to the field capacity.

Daejeon (Fig. 8c) is rainier than the other two stations (i.e., Jibyeon and Seoul). Being the soil type clay loam, even in this station the soil moisture in July and August is very close and sometimes higher than the field capacity (0.82).

Figure 7 represents the daily averaged values of the energy budget components (net radiation, sensible and latent heat fluxes, and soil conductive heat flux). The net radiation shows some variations (mainly as a result of the cloudiness), but its maxima and minima do not change appreciably during the entire season, oscillating approximately between 50 (cloudy days) and 180 W m^{-2} (sunny days).

The latent heat flux, before the onset of the precipitations, was lower than or comparable to the sensible heat flux (see Jibyeon in Fig. 7a and Daejeon in Fig. 7c, respectively) while becoming very large during

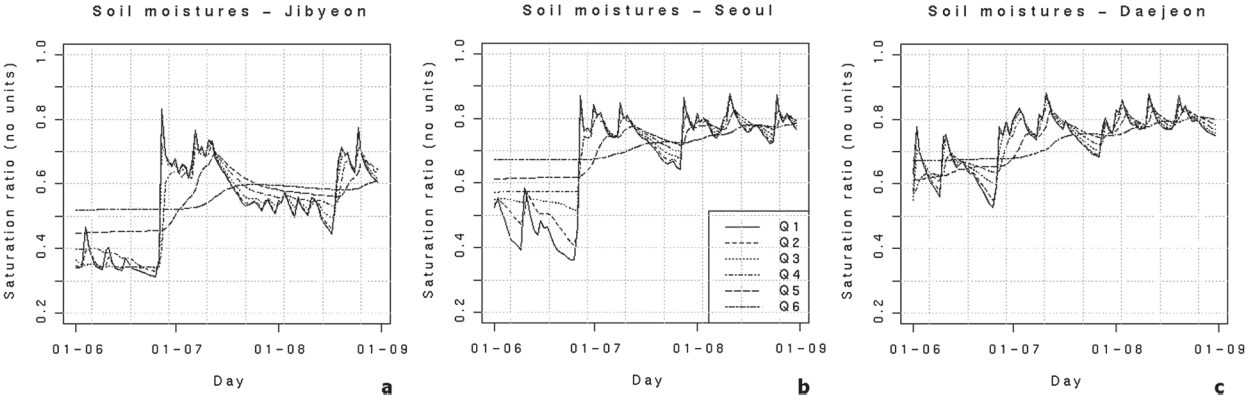

FIG. 8. Daily mean soil moisture of the upper five soil layers, expressed in units of saturation ratio, at (a) Jibyeon, (b) Seoul, and (c) Daejeon.

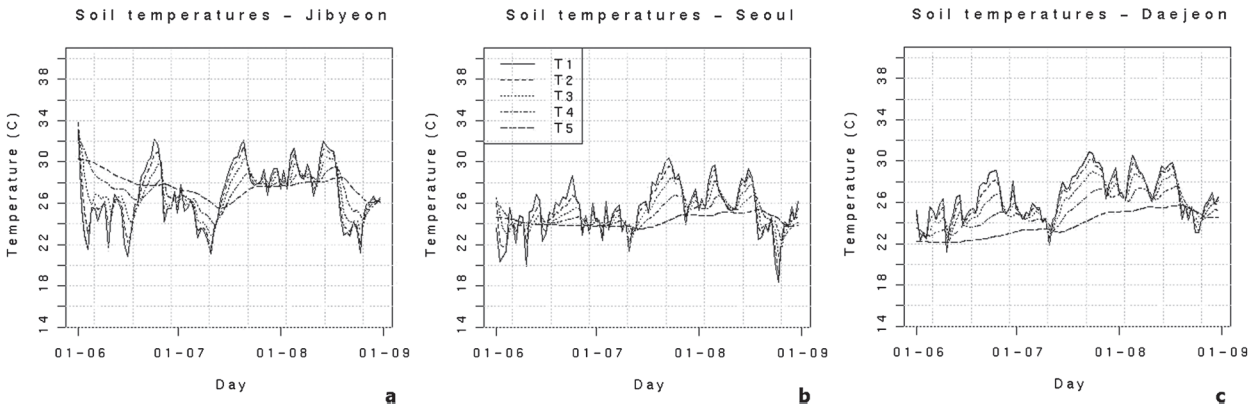

FIG. 9. Daily mean temperatures (°C) of the upper five soil layers at (a) Jibyeon, (b) Seoul, and (c) Daejeon.

the period of the precipitations, with oscillations between 50 and 150 W m^{-2}. On some clear sky days, the latent heat flux assumes values similar to those of the net radiation, and even higher on some cloudy days, thus indicating that the energy was absorbed from the ground surface.

The sensible heat flux, however, during the rainy season, is slightly superior to the soil–atmosphere heat flux, reaching the highest values in prolonged rainless periods (as in the mid-July).

The soil temperatures (Fig. 9), especially those in the first soil layer, cool off considerably (6°–8°C) during the rainfall events, when the soil thermal gradient also decreases because of the greater thermal conductivity of the wet soil. A common characteristic for each station is the presence of three distinct periods. Immediately before the onset of the precipitations, the surface soil temperatures grow considerably by 8°–10°C, exceeding 28°C (and also 30°C in Jibyeon). During the first period of intense rainfall (e.g., between the last third of June and the first third of July), there is a gradual cooling of soil surface of 6°–10°C. After 12 July, surface soil temperatures rise again by 7°–10°C in about 10 days. In the subsequent 25–30 days, surface soil temperatures show some oscillations keeping quasi-stationary values even with the precipitation events. Lastly, during the final 10–15 days of August, the last monsoon rainfalls produce a net cooling by 6°–10°C in the surface soil temperature, especially in Seoul.

In all stations, there exist two periods in which the soil temperatures reach very high values, sometimes exceeding 30°C, while the soil moistures show minimum values—the first period is between 20 and 25 June, and the second period is around 17 July. The soil temperatures of the deepest layer show behaviors similar to those of the surface layer, with progressively smoothed fluctuations. The analysis of the fifth-layer curve, whose center is located 1.15 m below the soil surface, shows clearly the propagation of the thermal wave in the deep soil.

b. Spatial variability in 2D maps

For the spatial variability, two-dimensional (2D) map analyses are performed. The 2D maps (Figs. 10–14) represent the territorial distribution over Korea of the monthly-mean or accumulated (for hydrologic quantities) values during summer (June–August) for net radiation, sensible and latent heat fluxes, and the first-layer soil moisture and temperature. The maps are drawn by interpolating the irregularly distributed station data with the kriging model and plotting with the isocontouring routines of R in polygonal representation (see section 2). In the discussion of the maps, the areas without observational stations (whose position is indicated by white and black dots in the maps) will not be taken into consideration, as the isocontouring is the result of a graphical artifice.

Figure 10 shows the monthly averaged net radiation. Generally, net radiation is larger in the extreme southwestern sector (including the island of Jeju), especially on the plain at the southern mouths of the southern MRs (such as the Naju and Gimhae plains), and smaller in the northwestern sector, where precipitation is also smaller. Western Korea has a weaker gradient than the eastern part, where net radiation is more uniform. A similar behavior is also present in the distribution of global radiation (not shown). The most significant geographic pattern is the area with low values in the Gyeonggi-do province, near Seoul, over the northwestern region. The net radiation is thus greater in the suburban areas than in the urban areas, especially in Seoul and its surroundings. In the urban areas, the soil has a greater albedo (as a result of the urban canopy) and the global radiation is lower (on average, about 20–30 W m^{-2} less than in the neighboring areas; not shown). The lower global

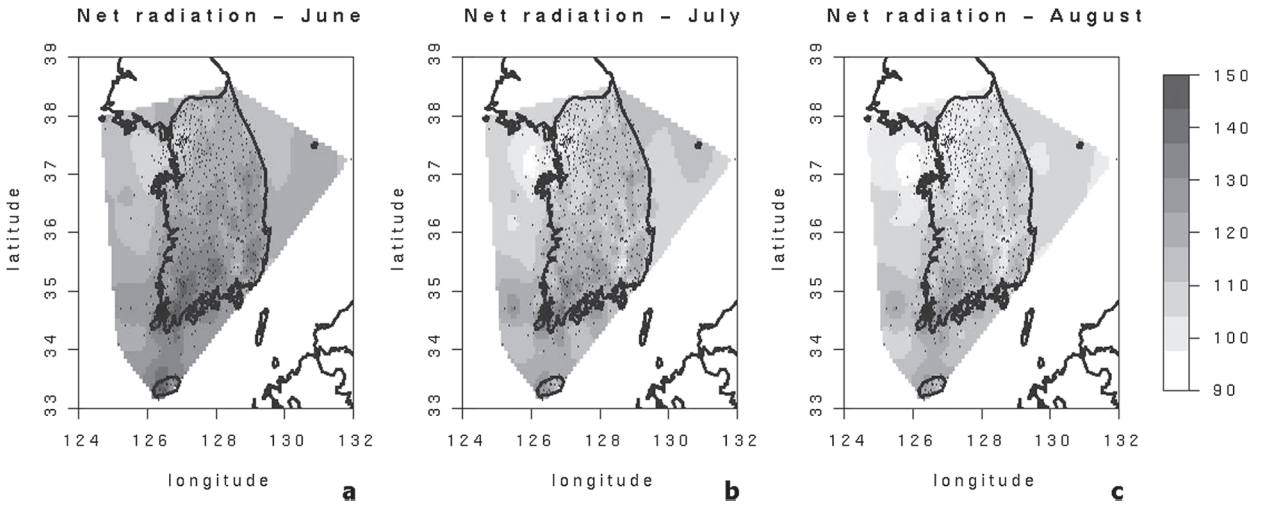

FIG. 10. Map of monthly-mean net radiation (W m^{-2}) for 2005 for (a) June, (b) July, (c) August. Black dots indicate the position of the stations. The gray areas without dots are not meaningful.

radiation can be explained by considering the larger cloudiness or the larger sky turbidity, which is in turn linked to the aerosol concentration increase. Near Seoul, there are many industries that could be responsible, together with the heavy traffic (Gyeonggi-do is the most populated region of Korea.), for the increase of pollution and aerosol concentration, which in turn could absorb the solar radiation and act as additional cloud condensation nuclei, thus favoring larger cloudiness. This hypothesis is confirmed by Chun et al. (2003), who found that severe cloudy and hazy air (haze) occurs in the afternoon in Seoul. In addition, Oke (1988), based on measurements from numerous cities, concluded that shortwave radiation received at the surface may be reduced by any amount between 1% and 15%, depending on the type of aerosols, meteorological conditions, among others.

A particular consideration can be reserved for Jeju, the major Korean island. During June and July, the western part of the island shows higher net radiation than the eastern part, while monthly precipitations (Fig. 3) are low and almost equally distributed over both sides of the island. The solar radiation (not shown) depicts a minimum in the central part of the island, where Mt. Halla (1950 m MSL), the highest peak of SK, favors higher cloudiness, and a maximum over the northern sector, perhaps downwind to Mt. Halla. Thus, the only parameter that could explain this difference in the net radiation is surface albedo, showing different values for different soil and land-use characteristics over the two sides of Mt. Halla.

The sensible heat flux (Fig. 11) is always larger over Jeju, on the extreme southwestern coasts (not in July), on the southeastern coasts, and on one island in the Gyeonggi Bay (west of Incheon). This is observed in all summer months, even if numerical values decrease from June to August. During June, all internal stations (and particularly those located over the Taebaek and Noryeong MRs) show the lowest values. The same pattern is present in July—the Gyeongsangbuk-do/Daegu region having values slightly higher than central zones—with numerical values about half compared to those in June. In August, there is the most regular distribution, with the minimum (almost null) in the Gangwon-do region, in the extreme northeast, and on the islands west of the Honam Plain. The numerical values are lower than those in July. In each month, coastal areas have higher values than the internal areas, and the Gyeonggi-do region (including Seoul) has a sensible heat flux always slightly higher than the surrounding areas.

The latent heat flux (Fig. 12) shows some common characteristics in all months. The maxima are located over the Jeollabuk-do and Jeollanam-do regions (except the Honam plain) in the southwestern Korea, spreading also on the coastal Gyeongsangnam-do region (extreme south). The minima are located in the Gyeonggi-do (Seoul) region and in some islands west of Incheon, where in June the latent and sensible heat fluxes are almost equal. Another minimum is observed in the mountainous Gyeongsangnam-do region (near Mt. Gaya, 1430 m MSL, at the south). In July and August, a secondary maximum of latent heat flux is evident over the Gwangju MR, at the extreme northeast. In August, the values of latent heat flux are slightly (much) higher than those in July (June), implying a large evapotranspiration. In some cloudless (cloudy) days, the latent heat

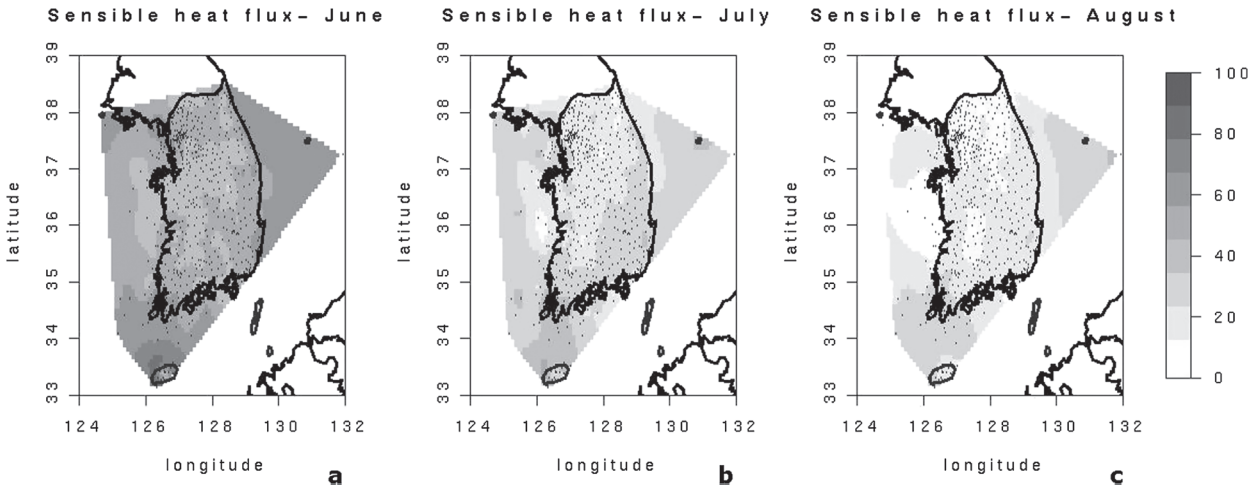

FIG. 11. Same of Fig. 10 but for sensible heat flux (W m^{-2}).

flux equals (exceeds) the net radiation, thus indicating that the soil thermal energy is used for evapotranspiration processes.

The surface soil moisture (expressed as a fraction of the porosity and shown in Fig. 13) is generally larger in the northwestern part of SK, and appears to be not strongly correlated with the precipitation itself. This is reasonable, as the evapotranspiration, the runoff, and the drainage (not shown) must also be considered. The central and southeastern areas show smaller soil moisture amount due to strong evaporation and lower precipitation. The northwestern area—from Gyeonggi-do to northern Chungcheongnam-do—as well as a small region near Mokpo show the surface soil moisture close to the field capacity during July and August, and the highest values in Korea during June. Notice that the area around Mokpo is the only zone in the southwestern Korea characterized by a clay loam soil type (Park et al. 2003). In the Gyeonggi-do region, the surface soil moisture is low in June but increases strongly in July and August. The maxima of surface soil moisture occur in the western areas of Jeollakbuk-do, where the greatest extension of (rice) paddy fields is located. The eastern coasts as well as the eastern side of Jeju show the lowest soil moistures. Therefore, it can be concluded that, over the Korean Peninsula in summer, the soil moisture pattern is closely related to the distribution of soil types, and that there are some deviations in isolated areas and times under the influence of the precipitation. This result is similar to that of Munro et al. (1998) in Australia and implies that the response of soil types to the drying factors (e.g., the hydrologic budget

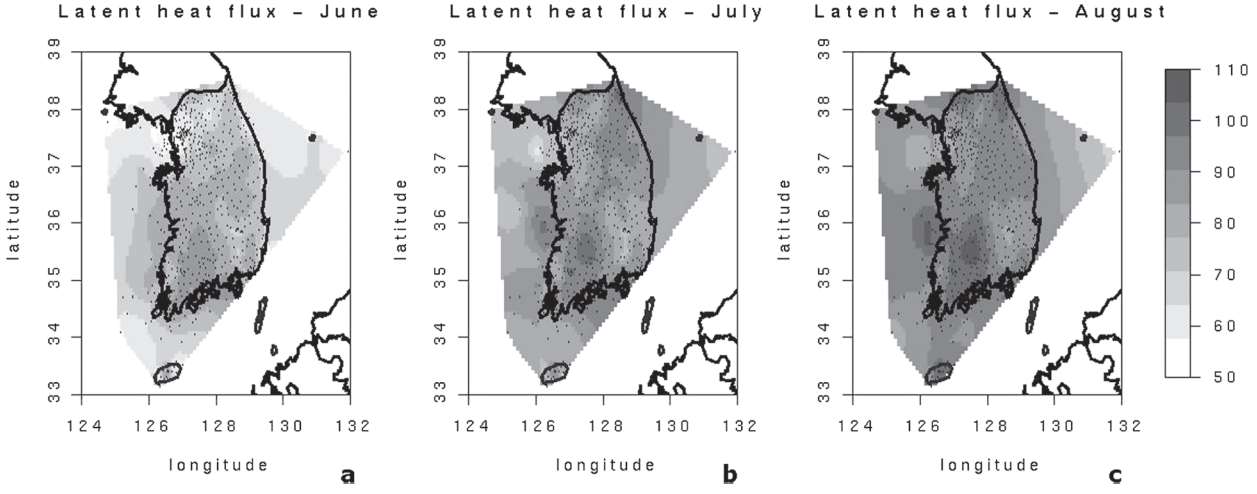

FIG. 12. Same of Fig. 10 but for latent heat flux (W m^{-2}).

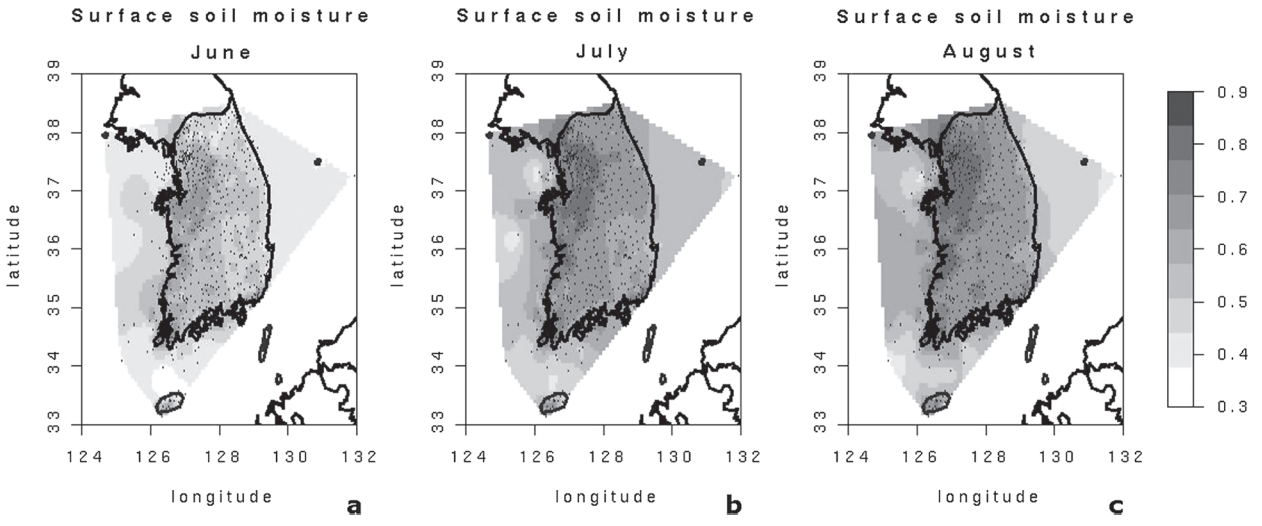

FIG. 13. Same of Fig. 10 but for soil moisture in the first layer, in units of saturation ratio.

components) is primarily responsible for the soil moisture status.

Regarding the surface soil temperatures, Fig. 14 shows the effect of topography (the highest stations are also the coldest) increasingly evident month by month. The coldest region is located over the Taebaek MR, on the northeast, whereas in the south there are two warm tongues separated by the Sobaek MR. The decrease of temperature with the elevation appears evident only for MRs higher than 1000 m MSL, whereas the lowest ranges do not show significant decreases, as in the case of the Noryeong MR (in the extreme southwest) and Charyeong MR (in the central part of the Korean Peninsula). Thus these low MRs appear to influence the local precipitation pattern but not the local temperature.

8. Conclusions

In this study, a series of analyses on the components of the energy and hydrologic budgets, and of the soil temperature and moisture calculated by the LSPM over 635 South Korean stations are carried out. The LSPM is validated over the main climatic areas in Korea by comparing some model-calculated variables with their corresponding observations. The results show that the LSPM is able to represent, with high degree of accuracy, the soil temperatures measured over the Korean territory. Although other datasets could eventually allow the comparison with other model outputs, our validation results indicate that the LSPM is capable of correctly simulating soil conditions during the monsoon season, in

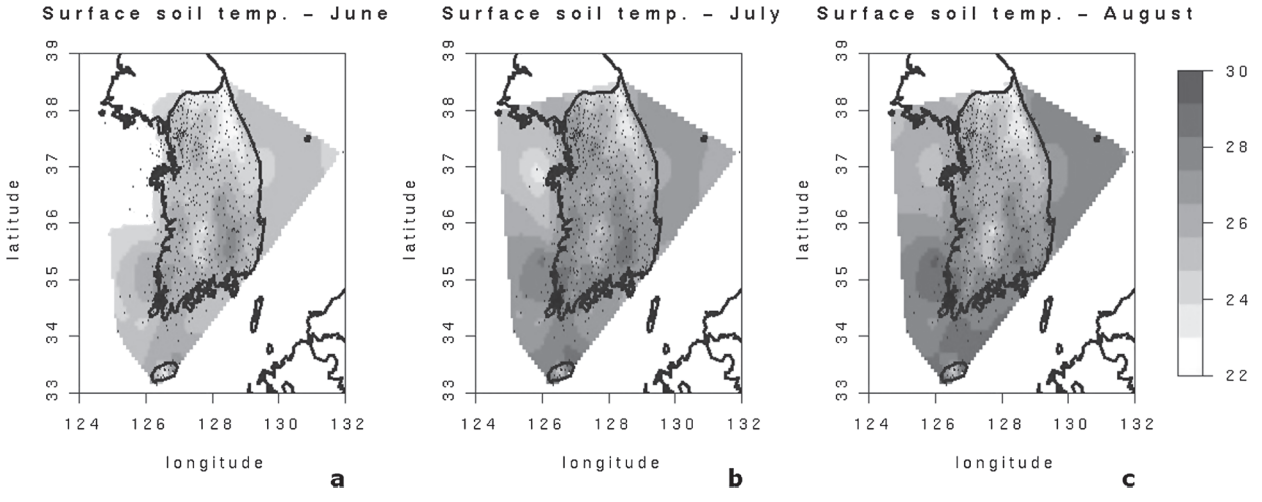

FIG. 14. Same of Fig. 10 but for soil temperature in the first layer (°C).

which the soil is very wet and the thermal conductivity is very high. The LSPM has been comprehensively tested by carrying out sensitivity experiments for the soil and vegetation characteristics. The soil and vegetation types turned out to be very sensitive during the monsoon season, and thus they were evaluated using the specific databases KLCV and Ecoclimap.

During the rainy season, the greater part of precipitation is stored in the soil because of the high values of hydraulic conductivity, and the soil moisture often exceeds the field capacity in the first layer of soil. This stored water is a sort of ''reservoir'' and, through its infiltration in the deep soil, constitutes the base for the vegetation life in the drier season successive to the monsoon. During the rainy season, in the days with no precipitations, the evapotranspiration is the dominant term of both energy and hydrologic budgets. The spatial distribution of variables shows that the mountainous areas, with high precipitation, have very strong evapotranspiration to consume the soil moisture efficiently. The southeastern areas with low precipitation are also the warmest areas of Korea.

The urban and suburban areas of Seoul, and generally the entire Gyeonggi-do region, show lower values of soil moisture, solar and net radiation, and evapotranspiration, and higher values of sensible heat flux and soil temperature (relatively to neighboring areas). With these characteristics this area is considered to have a peculiar microclimate. Because of the abundance of stations in this area, a possible future analysis could be carried out over the most industrialized and populated zone of Korea.

The results of the LSPM in this study, applied to the Korean monsoon environment, can be regarded as very preliminary. However, some of the findings are quite new and interesting. The soil moisture is not directly linked to the precipitation only but to all the components of the hydrologic budget (which in turn depends on soil and vegetation type). In addition, the types of vegetation and soil are crucial to estimate accurately the land surface variables, and thus are important in improving our understanding on the land–atmosphere exchange processes and the short-term weather forecasting as well as the long-term climatic simulations. Because most of the land surface variables estimated in this study have some difficulty in getting proper observation (for the validation of model results), a long-term database of such variables obtained from this kind of study will be essential and useful for assessing future climate scenarios in Korea.

Acknowledgments. We are grateful to Prof. M. S. Suh of Kongju National University for providing the KLCV dataset. This work is partly supported by the Korea Foundation for International Cooperation of Science and Technology (KICOS) through a grant (K20713000007-08B0100-00710) provided by the Korean Ministry of Education, Science and Technology (MEST) for 2007–09 under the Executive Programme for the Scientific and Technological Cooperation between the Italian Republic and the Republic of Korea in the frame of the project Climate Change and its Impact on Land Surface Processes and Vegetations at Regional Scale between the Faculty of Science of the University of Torino, Italy, and the Severe Storm Research Center of the Ewha Womans University, Seoul, Korea. It is also partly supported by the Ministry of Environment, Korea, under the National Comprehensive Measures against Climate Change Program (Grant 1700-1737-322-210-13).

REFERENCES

Balsamo, G., 1999: Initialization of surface data in numerical models of atmospheric circulation (in Italian). M.S. thesis, Dept. of Physics, University of Turin, 255 pp.

Cassardo, C., 2006: The land surface process model (LSPM) version 2006: The complete manual. Department of General Physics, ''Amedeo Avogadro'' University of Turin Internal Rep. 012006, 61 pp.

——, J. J. Ji, and A. Longhetto, 1995: A study of the performances of a land surface process model (LSPM). *Bound.-Layer Meteor.,* **72,** 87–121.

——, P. M. Ruti, C. Cacciamani, A. Longhetto, T. Paccagnella, and A. Bargagli, 1997: CLIPS experiment. First step: Model intercomparison and validation against experimental data. MAP Newsletter, No. 7, MeteoSwiss MAP Programme Office, Zurich, Switzerland, 74–75.

——, E. Carena, and A. Longhetto, 1998: Validation and sensitivity tests on improved parametrizations of a land surface process model (LSPM) in the Po Valley. *Nuovo Cimento,* **21C,** 189–213.

——, G. P. Balsamo, R. Pelosini, C. Cacciamani, D. Cesari, T. Paccagnella, and A. Longhetto, 1999: Initialization of soil parameters in LAM: CLIPS experiment. MAP Newsletter, No. 11, MeteoSwiss MAP Programme Office, Zurich, Switzerland, 26–27.

——, N. Loglisci, D. Gandini, M. W. Qian, G. Y. Niu, P. Ramieri, R. Pelosini, and A. Longhetto, 2002a: The flood of November 1994 in Piedmont, Italy: A quantitative analysis and simulation. *Hydrol. Processes,* **16,** 1275–1299.

——, G. P. Balsamo, C. Cacciamani, D. Cesari, T. Paccagnella, and R. Pelosini, 2002b: Impact of soil surface moisture initialization on rainfall in a limited area model: A case study of the 1995 South Ticino flash flood. *Hydrol. Processes,* **16,** 1301–1317.

——, D. Bertoni, S. Ferrarese, R. Forza, A. Longhetto, and M. W. Qian, 2002c: Application of a land surface model (LSPM) on ice shelf of Antarctica. *Proc. 11th Int. Symp. on Acoustic Remote Sensing (ISARS 2002),* Rome, Italy, International Society for Acoustic Remote Sensing, 123–126.

——, N. Loglisci, and M. Romani, 2005: Preliminary results of an attempt to provide soil moisture datasets in order to verify numerical weather prediction models. *Nuovo Cimento,* **28C,** 159–171.

——, ——, G. Paesano, D. Rabuffetti, and M. W. Qian, 2006a: The hydrological balance of the October 2006 flood in Piedmont,

Italy: Quantitative analysis and simulation. *Phys. Geogr.,* **27,** 1–24.

——, S. Ferrarese, A. Longhetto, M. G. Morselli, and G. Brusasca, 2006b: A reanalysis of the atmospheric boundary layer field experiment (SPCFLUX93) at San Pietro Capofiume (Italy). *Nuovo Cimento,* **29C,** 565–597.

——, L. Mercalli, and D. Cat Berro, 2007: Characteristics of the summer 2003 heat wave in Piedmont, Italy, and its effects on water resources. *J. Korean Meteor. Soc.,* **43,** 195–221.

Chen, F., and Coauthors, 1996: Modeling of land-surface evaporation by four schemes and comparison with FIFE observations. *J. Geophys. Res.,* **101** (D3), 7251–7268.

Chun, Y.-S., J.-Y. Lim, and B.-Y. Choi, 2003: The features of aerosol in Seoul by Asian dust and haze during springtime from 1988 to 2002. *J. Korean Meteor. Soc.,* **39,** 459–474.

Clapp, R. B., and G. M. Hornberger, 1978: Empirical equations for some soil hydraulic properties. *Water Resour. Res.,* **14,** 601–604.

Cressie, N. A. C., 1991: *Statistics for Spatial Data*. Wiley, 920 pp.

Dirmeyer, P. A., 2000: Using a global soil wetness dataset to improve seasonal climate simulation. *J. Climate,* **13,** 2900–2922.

——, F. J. Zeng, A. Ducharne, J. C. Morrill, and R. D. Koster, 2000: The sensitivity of surface fluxes to soil water content in three land surface schemes. *J. Hydrometeor.,* **1,** 121–134.

Douville, H., and F. Chauvin, 2000: Relevance of soil moisture for seasonal climate predictions: A preliminary study. *Climate Dyn.,* **16,** 719–736.

Ek, M., and R. H. Cuenca, 1994: Variation in soil parameters: Implications for modeling surface fluxes and atmospheric boundary layer development. *Bound.-Layer Meteor.,* **70,** 369–383.

Eltahir, E. A. B., 1998: A soil moisture feedback mechanism. *Water Resour. Res.,* **34,** 765–776.

FAO, 1988: FAO/UNESCO soil map of the world. FAO World Soil Resources Rep. 60, 119 pp.

Feng, J. C., X. M. Liu, C. Cassardo, and A. Longhetto, 1997: A model of plant transpiration and stomatal regulation under the condition of waterstress. *J. Desert Res.,* **17,** 59–66.

Koster, R. D., and M. J. Suarez, 2001: Soil moisture memory in climate models. *J. Hydrometeor.,* **2,** 558–570.

Malla Thakuri, B., 2007: Estimation of land surface parameters in the Korean Peninsula during summer time using the land surface process model (LSPM). M.S. thesis, College of Engineering, Ewha Womans University, 108 pp.

Masson, V., J.-L. Champeaux, F. Chauvin, C. Meriguet, and R. Lacaze, 2003: A global database of land surface parameters at 1-km resolution in meteorological and climate models. *J. Climate,* **16,** 1261–1282.

Munro, R. K., W. F. Lyons, Y. Shao, M. S. Wood, L. M. Hood, and L. M. Leslie, 1998: Modelling land surface–atmosphere interactions over the Australian continent with an emphasis on the role of soil moisture. *Environ. Modell. Software,* **13,** 333–339.

Namias, J., 1952: The annual course of month-to-month persistence in climatic anomalies. *Bull. Amer. Meteor. Soc.,* **33,** 279–285.

Oke, T. R., 1988: The urban energy balance. *Prog. Phys. Geogr.,* **12,** 471–508.

Park, Y. H., K. S. Lee, H. Y. Lee, I. Son, and J. R. Lee, Eds., 2003: *Atlas of Korea*. Sung Ji Mun Hwa Co. Ltd., 160 pp.

Priolo, D., 2007: Energy and hydrologic budgets in the surface layer during the monsoon season in Korea (in Italian). M.S. thesis, Dept. of Mathmematical, Physical and Natural Sciences, University of Turin, 168 pp.

Qian, M. W., N. Loglisci, C. Cassardo, A. Longhetto, and C. Giraud, 2001: Energy and water balance at soil-interface in a Sahelian region. *Adv. Atmos. Sci.,* **18,** 897–909.

Reed, C. D., 1925: Monthly forecasts by correlation: June, a key month. *Mon. Wea. Rev.,* **53,** 249–251.

Rind, D., 1982: The influence of ground moisture conditions in North America on summer climate as modeled in the GISS GCM. *Mon. Wea. Rev.,* **110,** 1487–1494.

Robock, A., K. Y. Vinnikov, G. Srinivasan, J. K. Entin, S. E. Hollinger, N. A. Speranskaya, S. Liu, and A. Namkhai, 2000: The Global Soil Moisture Data Bank. *Bull. Amer. Meteor. Soc.,* **81,** 1281–1299.

Ruti, P. M., C. Cassardo, C. Cacciamani, T. Paccagnella, A. Longhetto, and A. Bargagli, 1997: Intercomparison between BATS and LSPM surface schemes, using point micrometeorological data set. *Beitr. Phys. Atmos.,* **70,** 201–220.

Shao, Y., and A. Henderson-Sellers, 1996: Modeling soil moisture: A project for intercomparison of land surface parameterization schemes phase 2(b). *J. Geophys. Res.,* **101,** 7227–7268.

Shukla, J., and Y. Mintz, 1982: Influence of land-surface evapotranspiration on the earth's climate. *Science,* **215,** 1498–1501.

Takao, Y., K. Fujio, and E. Seita, 2001: Numerical study on the baiu front genesis by heating contrast between land and ocean. *J. Meteor. Soc. Japan,* **79,** 671–686.

Wilson, M. F., and A. Henderson-Sellers, 1985: A global archive of land cover and soils data for use in general circulation climate models. *J. Climatol.,* **5,** 119–143.

Xue, Y., P. J. Sellers, F. J. Zeng, and C. A. Schlosser, 1997: Comments on ''Use of midlatitude soil moisture and meteorological observations to validate soil moisture simulations with biosphere and bucket models.'' *J. Climate,* **10,** 374–376.

Yan, H., and R. A. Anthes, 1988: The effect of variations in surface moisture on mesoscale circulations. *Mon. Wea. Rev.,* **116,** 192–208.

Yeh, T.-C., R. T. Wetherald, and S. Manabe, 1984: The effect of soil moisture on the short-term climate and hydrology change—A numerical experiment. *Mon. Wea. Rev.,* **112,** 474–490.